王丹, 付勇. 湖南铜山岭花岗闪长岩中榍石微区原位 Nd 同位素和微量元素组成及其岩石成因的指示意义[J]. 岩矿测试, 2023,42(2):282-297. doi: 10.15898/j.cnki.11-2131/td.202202230031.
WANG Dan, FU Yong. Petrogenesis of the Mesozoic Tongshanling Granodiorite in Southern Hunan Province, South China: Clues from *in-situ* Nd Isotopes and Elements of the Titanite[J]. Rock and Mineral Analysis, 2023, 42(2): 282-297. doi: 10.15898/j.cnki.11-2131/td.202202230031.

湖南铜山岭花岗闪长岩中榍石微区原位 Nd 同位素和微量元素组成及其岩石成因的指示意义

王丹, 付勇*
(贵州大学资源与环境工程学院, 贵州 贵阳 550025)

摘要: 与热液矿床形成有关的花岗质岩石普遍遭受热液蚀变,且全岩成分仅代表均一化某一时间点的信息,采用全岩成分分析难以有效地揭示花岗质岩石的形成与演化。花岗质岩石中副矿物稳定不容易蚀变,近年原位测试技术的快速发展和日趋成熟,可以准确获取副矿物原位元素和同位素组成,通过副矿物元素和同位素组成可以有效地揭示岩浆来源和演化信息,显著提高了岩浆作用过程的空间分辨率,成为探讨岩石成因的新手段。本文以湘南与铜铅锌多金属成矿密切相关的铜山岭岩体为研究对象,利用电子探针(EPMA)、激光剥蚀等离子体质谱(LA-ICP-MS)和激光剥蚀多接收等离子体质谱(LA-MC-ICP-MS)等原位测试技术,对花岗闪长岩和暗色包体两类岩石样品中的副矿物榍石开展了原位元素和 Nd 同位素分析。结果表明:所有榍石中 Al+Fe 与 Ti 具有明显的负相关关系且稀土元素含量较高,稀土元素与 Al 和 Fe 一起主要通过 $(Al,Fe^{3+})+REE=Ti^{4+}+O^{2-}$ 方式替换榍石的 Ti 位和 Ca 位而进入晶格。球粒陨石标准化稀土配分模式上,大部分榍石显示 Eu 正异常。榍石中微量元素对 Zr/Hf、Nb/Ta、Y/Ho 比值变化范围分别为 21.0~31.5、10.4~13.9、27.4~35.0,未发生明显分异。暗色包体中榍石的 $\varepsilon_{Nd}(t)$ 值为-3.5~-8.9,平均值为-7.2±2.4,花岗闪长岩中榍石的 $\varepsilon_{Nd}(t)$ 值为-5.4~-9.9,平均值为-6.9±2.4,所有榍石中 Nd 同位素组成均一且具有一致的负的初始 Nd 同位素组成,与华南大陆中下地壳 Nd 同位素演化趋势一致。元素地球化学特征表明,榍石中微量元素只与其晶体结构有关,不受热液蚀变作用的影响,能有效地示踪岩浆起源和性质。通过元素和同位素地球化学特征研究,本文认为铜山岭花岗质岩浆具有高温、高氧逸度特征,很可能由镁铁质角闪岩相中下地壳脱水熔融产生的水不饱和岩浆形成。

关键词: LA-MC-ICP-MS; 原位同位素分析; Nd 同位素; 微量元素; 榍石; 花岗闪长岩; 湘南地区

要点:

(1) 铜山岭榍石中元素组成受晶体结构控制,其微区原位元素特征记录岩浆初始信息。

(2) 铜山岭花岗闪长质岩浆具有高温、高氧逸度特征。

(3) 铜山岭花岗闪长岩由中下地壳脱水熔融产生的水不饱和岩浆形成。

中图分类号: O657.63; O562.6 **文献标识码**: A

花岗质岩岩石是地球大陆地壳有别于其他行星的重要标志,且与大量的岩浆-热液矿床在时空和成因上密切相关[1-3],有关花岗质岩石的形成与演化一直是地质学者研究的热点。花岗质岩石主要矿

收稿日期: 2022-02-23; **修回日期**: 2022-08-20; **接受日期**: 2022-12-07
基金项目: 贵州省创新人才基地项目(RCJD-2018)
第一作者: 王丹,硕士研究生,研究方向:花岗岩成岩成矿作用。E-mail: 273705742@qq.com。
通信作者: 付勇,博士,教授,研究方向:沉积学和沉积矿床学。E-mail: Byez1225@126.com。

物组成比较简单,一般由长石、云母和石英组成,但有关其岩石起源与演化一系列问题一直存在激烈的争议。绝大多数情况下,人们大多借助元素和同位素地球化学来限定花岗质岩石成因,如以往常采用全岩的 Sr、Nd、Pb 等放射成因同位素来进行示踪,遗憾的是这些同位素在很多情况下难以对花岗质岩浆的形成与演化提供明确的制约[4-5]。这是因为全岩同位素示踪存在三个方面的局限性:①岩浆在侵位过程当中如果发生了多次岩浆改造(Modification),如岩浆混合、围岩同化混染和结晶分异等,Sr-Nd 同位素测定值代表的是均一化后某一个时间点(snapshot)的信息,无疑会隐藏许多岩浆来源的信息[6];②全岩放射成因同位素能够较合理地监测到古老地壳和软流圈地幔物质,但很难监测到年轻物质的具体混入量,因为后者的放射成因子体同位素难以准确测量,而且年轻的幔源岩石或者岛弧火山岩在参与花岗岩形成之前如果遭受热液蚀变,Sr 同位素只有少量变化,而 Nd 和 Pb 同位素没有变化[4],故难以准确地判断其源岩性质;③使用全岩放射成因同位素分析问题时,我们通常假定岩石中各矿物相具有相同的来源并且保持同位素平衡,但近年来人们发现一些矿物与其寄主岩石在同位素组成上可以存在很大差别[7]。因此,仅借助全岩放射成因同位素来示踪岩浆来源,许多详细的岩浆来源信息及源岩性质变化细节不能被有效地揭露出来,况且与成矿有关的花岗质岩石常普遍遭受不同程度的热液蚀变,这就给用全岩化学成分限定岩浆起源与形成过程带来了更大难度。

为了攻克这个难题,越来越多的研究者试图利用花岗岩中矿物的元素和同位素来揭示岩石成因和演化过程,但由于侵入岩缓慢的冷却过程,亚固相线下大部分矿物的化学成分得到重新平衡,许多详细的岩石成因信息已经丢失[8]。而副矿物具有难熔、惰性和化学性质稳定等特征,一般不易受后期热事件的影响[8-9],即使在特定的条件下发生改变,也能通过结构及成分有效地辨别出来[10-12]。同时,副矿物中含有岩石中大部分高场强元素和稀土元素,这些元素和相关同位素在副矿物中扩散速率缓慢,其结晶过程随着岩浆物理化学条件的改变而表现出不同的结构与地球化学特征,甚至能保存元素和同位素环带,被视为岩浆来源和演化过程的监测器,最大限度地保留了岩浆来源与演化过程的地球化学指纹[12-13]。近年来,随着激光剥蚀电感耦合等离子体质谱(LA-ICP-MS)和激光剥蚀多接收等离子体质谱(LA-MC-ICP-MS)等微区原位分析技术的快速发展和日趋成熟,使得对副矿物进行原位成分测定、获得高精度微量元素和同位素组成得以实现,极大地促进了副矿物在岩石成因中的应用[13-14]。如 Bruand 等[13]通过对副矿物锆石、磷灰石和榍石进行了原位氧同位素分析,识别出古老花岗岩受后期变质作用的影响,而全岩分析无法揭示出来。越来越多的研究表明,副矿物榍石[CaTi(SiO_4)O]微区原位元素和 Nd 同位素组成,也能够详细揭示岩浆来源和岩浆变化的细节,可显著提高岩浆作用过程的空间分辨率,是探讨岩浆来源与岩石成因的新的有效手段,避免了利用全岩分析为我们探讨花岗岩类成因带来的困扰[15-17,14]。

湘南构造岩浆带是华南地区花岗质岩浆活动的重要组成部分,发育有多个高钾钙碱性花岗闪长质小岩体,如水口山、宝山和铜山岭等,这些闪长质小岩体主要形成于 155~160Ma[18-19],在时空和成因上与铜铅锌多金属成矿密切相关,普遍遭受了不同程度的热液蚀变作用[19-21]。以往基于全岩元素和 Sr-Nd-Pb 同位素分析,先后提出壳-幔混合成因、残留体再造及中下地壳脱水熔融等多种不同成因模型[22-23],有关这些花岗闪长质岩体的源区特征及岩浆性质一直存在非常大的争议。本文以铜山岭岩体为对象,在详细的野外和镜下观察基础上,采用电子探针(EPMA)、激光剥蚀等离子体质谱(LA-ICP-MS)技术对暗色包体和花岗闪长岩两种岩石类型中榍石的主量、微量元素进行原位分析,采用激光剥蚀多接收等离子体质谱(LA-MC-ICP-MS)技术分析两类样品中榍石的原位 Nd 同位素组成,准确限定花岗闪长质岩石形成的源区特征和岩浆物理化学性质,为深入理解该地区花岗闪长质岩石成因及其大规模铜铅锌多金属成矿机制提供重要支撑。

1　地质背景

湘南位于华夏地块和扬子地块的结合部位,其东为华夏地块,西为扬子地块,是一个极富特色的铜铅锌多金属成矿密集区(图 1a)[24-25]。该地区主要出露的地层为古生界灰岩、碎屑岩[26]。岩浆作用强烈,花岗闪长质小岩体成带状密集分布,区域上自北向南分布的水口山、宝山、铜山岭是该地区铜铅锌多金属成矿有关的花岗闪长质小岩体的典型代表。

铜山岭岩体位于湘东南地区南部,由Ⅰ、Ⅱ、Ⅲ三个小岩体组成,近东西向分布,总面积 12km^2(图 1b)。该岩体侵入于寒武纪浅变质岩、泥盆纪海相碳酸盐岩

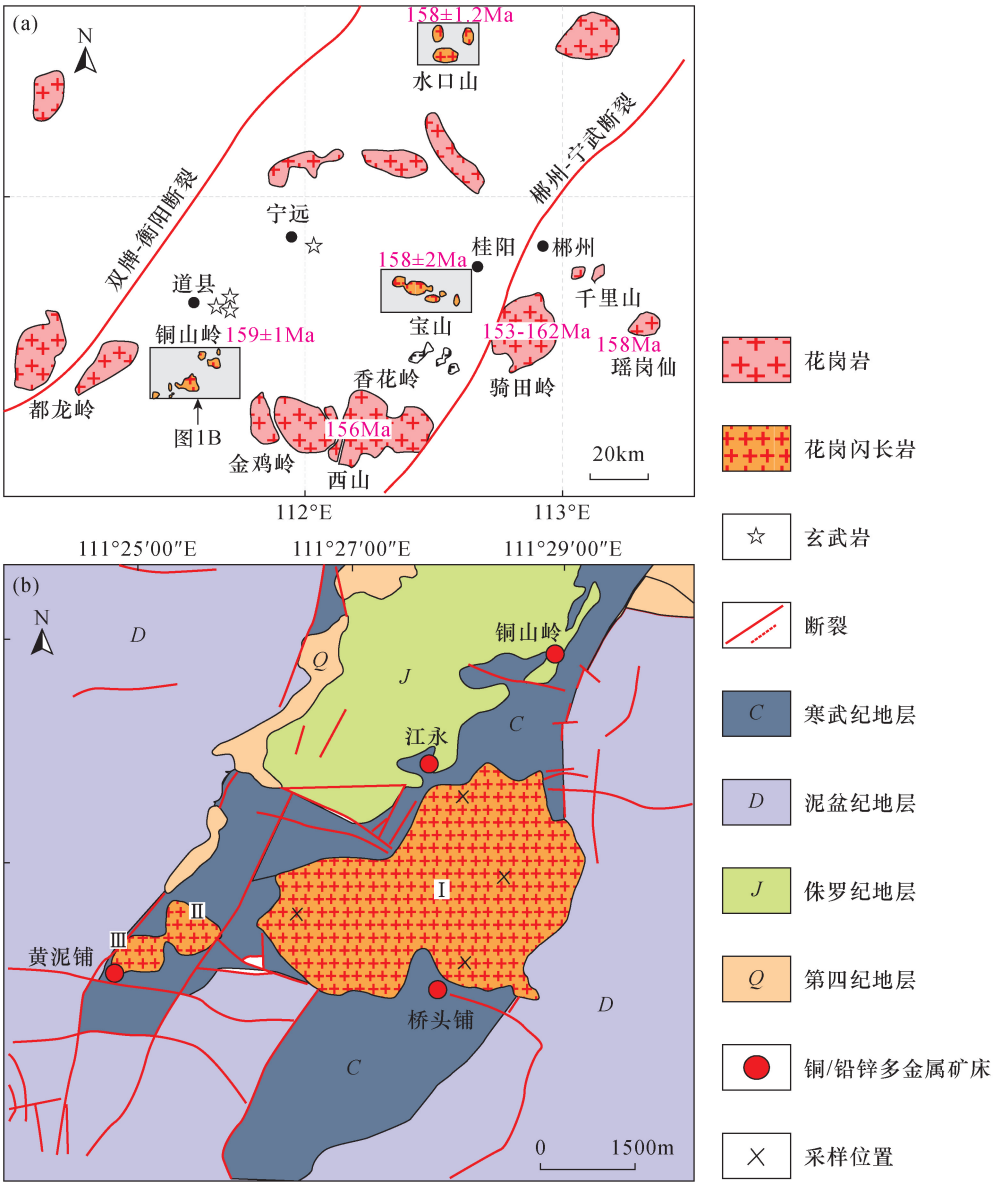

图 1　(a)湘南地区地质简图和(b)铜山岭岩体分布图(据文献 Wang 等[24]和卢友月等[25]修改)。湘东南的花岗闪长质侵入体位于华夏和扬子地块的结合部位,铜山岭岩体位于湘东南的南部,由Ⅰ、Ⅱ、Ⅲ等 3 个小岩体组成,本次研究的样品采自Ⅰ号岩体

Fig. 1　(a) The simplified geological map of southern Hunan Province and (b) the distribution of the Tongshanling granitic pluton (modified from Wang, et al.[24] and Lu, et al.[25]). Granodioritic pluton in southeast Hunan Province (South China) emplaced at the junction between Cathaysia and Yangtze bocks. The Tongshanling pluton is located in the south of southeast Hunan Province, and is composed of three small plutons Ⅰ, Ⅱ and Ⅲ. The studied samples were collected from No. Ⅰ pluton.

夹碎屑岩地层中,形成年龄为 159±1Ma[18]。岩体周边分布一系列铜铅锌多金属矿床(点),自北向南有铜山岭矽卡岩型-热液脉型铜多金属矿床、江永矽卡岩型银铅锌矿床、桥头铺矽卡岩型铜钼多金属矿床(图 1b)。前人通过年代学、同位素(S、Pb、C)及流体包裹体研究,大多认为这些矿床与铜山岭岩体在时空和成因上密切相关[21,25,27-28]。

2　实验部分

2.1　实验样品

本次研究的所有样品均采自铜山岭Ⅰ号岩体,岩性主要为角闪石黑云母花岗闪长岩(图 2a),主要矿物组成为角闪石、黑云母、长石和石英,角闪石一般呈棕色和浅绿色(图 2),局部可见有明显的蚀变特征。岩体中发育有大量的铁镁质暗色包体

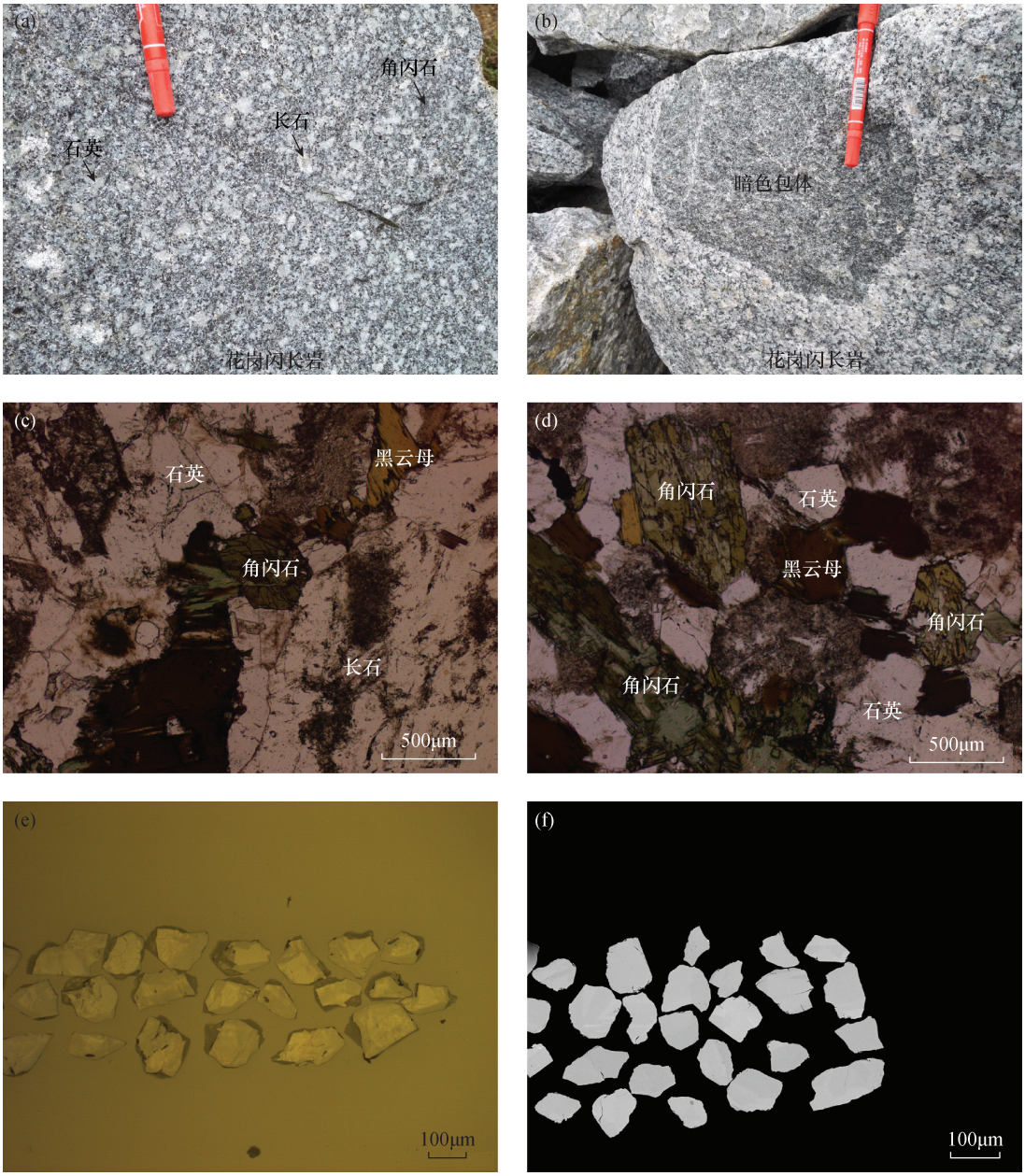

a—花岗闪长岩的主要矿物组合; b—花岗闪长岩中暗色包体; c—代表性花岗闪长岩镜下照片; d—角闪石镜下特征; e—透射光下榍石照片; f—榍石的背散射电子图像。

图 2　铜山岭岩体岩性特征和暗色包体照片及榍石透射光和背散射电子图像。铜山岭岩体中的花岗闪长岩主要由角闪石、长石、石英和黑云母组成。榍石在反射光和背散射电子图像中没有显示出明显的成分环带

Fig. 2　Characteristics of mafic microgranular enclave and hosted granodiorite, and photomicrographs of accessory mineral titanite. a—The major mineral assemblages of granodiorite; b—The mafic microgranular enclave hosted by granodiorite; c—Photomicrograph of the representative granodiorite; d—Photomicrograph of amphibole; e—Photomicrograph of titanite under transmission light; f—Black scatter electric image of titanite. The granodiorites are mainly composed of amphibole, feldspar, quartz, and biotite. Accessory mineral titanite grains in the MME and host granodiorite of the Tongshanling granitic pluton show little or no intra-grain concentric zoning in transmission and BSE images.

如图 2b 所示。主要由角闪石和黑云母等暗色矿物组成。

本文对花岗闪长岩和暗色包体样品进行粉碎后采用电磁法分选榍石,将分选的榍石颗粒制成环氧树脂靶,然后对榍石进行抛光处理,之后对榍石进行透反射光和背散射照相(图 2 中 e,f),检查榍石的内部结构,选择无裂痕、无微小矿物包裹体和表面平整的区域进行激光原位分析。

2.2　分析方法

2.2.1　榍石主量元素分析

榍石主量元素利用 EPMA 进行分析,在中国科学院地球化学研究所矿床地球化学国家重点实验室完成,仪器型号为日本电子生产的 JXA8530F-plus 型场发射电子探针。仪器工作条件为:加速电压 25kV,加速电流 10nA,束斑 5μm。采用自然界和人工合成国际标样对榍石中元素进行校正,用 Kaersutite 角闪石国际标样校正榍石的 Na、K、Mg、Al、Si、Ca、Mn 和 Fe 等元素的含量,磷灰石和金红石标样分别用来校正榍石中 F 和 Ti 的含量。元素特征峰测试时间为 10s,背景测试时间为 5s,所有测试数据均进行了 ZAF 校正处理。

2.2.2　榍石原位微量元素分析

榍石微量元素分析实验在中国科学院地球化学研究所矿床地球化学国家重点实验室利用 LA-ICP-MS 完成。激光剥蚀系统为 GeoLasPro 193nm ArF 准分子激光器,电感耦合等离子体质谱为 Agilent 7900。激光剥蚀过程中采用氦气为载气,氩气为补偿气,并加入少量氮气提高灵敏度,三者在进入 ICP 之前通过一个 T 形接头混合。样品仓为标配的剥蚀池,其中加入树脂制作的模具来获得一个较小体积的取样空间,以降低记忆效应,提高冲洗效率。分析过程中,激光工作参数频率为 5Hz,能量密度 5J/cm^2,束斑 44μm,分析点靠近电子探针点的位置,每个样品的总测试时间为 90s,采集背景信号 15s,样品剥蚀时间 60s,冲洗管路和样品池时间 15s。在测试之前用美国地调局研制的硅酸盐玻璃 NIST610 对 ICP-MS 性能进行优化,使仪器达到最佳的灵敏度和电离效率(U/Th≈1)、尽可能小的氧化物产率(ThO/Th<0.3%)和低的背景值。微量元素含量校正、仪器灵敏度漂移校正等都采用 ICPMSDateCal 软件处理,以对应点电子探针获得的 Ca 含量作为内标,标准物质 NIST610 和 NIST612 玻璃作为外标进行数据校正,微量元素分析的准确度优于 10%。

2.2.3　榍石原位 Sm-Nd 同位素分析

榍石 Sm-Nd 同位素分析实验在中国科学院地球化学研究所矿床地球化学国家重点实验室利用 LA-MC-ICP-MS 完成。激光剥蚀系统是澳大利亚瑞索公司生产的 RESOlution-155 ArF193-nm,多接收电感耦合等离子体质谱仪是英国 Nu 公司生产的 Nu Plasma Ⅲ。分析过程中,激光的束斑 72μm,剥蚀频率 6Hz,能量密度 6J/cm^2。使用^{144}Sm/^{147}Sm = 0.205484 和^{146}Nd/^{144}Nd=0.7129 分别校正 Sm 同位素和 Nd 同位素的质量歧视[29]。利用^{144}Sm/^{149}Sm = 0.22332 校正^{144}Sm 对^{144}Nd 的同质异位数干扰[30]。榍石标样 BLR-1 作为外标校正^{147}Sm/^{144}Nd 的质量歧视和元素分馏。实验测得的 4 个监控标样 MAD、Otter Lake、LAP 和 SAP 的^{143}Nd/^{144}Nd 比值分别为 0.511352±0.000008、0.511956±0.000008、0.511355±0.000015、0.511011±0.000007,与相应样品的^{143}Nd/^{144}Nd 参考值在误差范围内基本一致(MAD:0.511322±0.000053、Otter Lake:0.512940±0.000009、LAP:0.512352±0.000024、SAP:0.511007±0.000030)[17]。

3　榍石微区原位元素和同位素分析结果

3.1　榍石主量和微量元素特征

榍石主量、微量元素含量分别见表 1 和表 2。

分析结果显示,铜山花岗闪长岩及暗色包体中榍石的主量元素变化范围基本一致,SiO_2 为 31.0%~31.7%,Al_2O_3 为 1.81%~5.61%,CaO 为 29.0%~30.0%,TiO_2 为 30.6%~38.2%,FeO 为 0.184%~0.606%,F 为 0.48%~1.84%。对榍石原位微量元素分析显示,单个样品的微量元素含量变化范围不大,没有明显的成分环带。两类样品中榍石的稀土元素总量变化范围较大,为 67~1498μg/g,但二者稀土配分模式存在一定差别(图 3)[31],暗色包体中

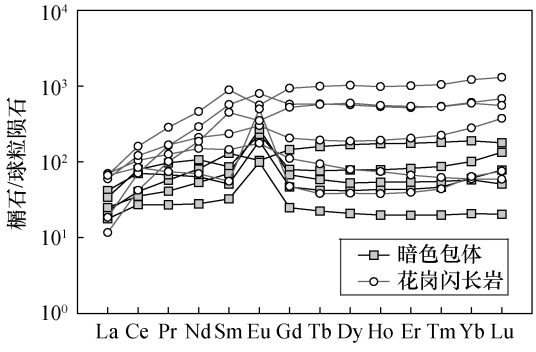

图 3　铜山岭榍石稀土元素配分模式图,暗色包体中榍石的稀土含量低于花岗闪长岩中榍石的稀土含量并具有明显的正 Eu 异常,而花岗闪长岩中的榍石显示出弱的正 Eu 或者负 Eu 异常。球粒陨石标准化数据据 Sun 和 McDonough[31]

Fig. 3　Chondrite-normalized REE patterns for titanite from the Tongshanling granitic pluton. Titanite from MME is characterized by Eu positive anomaly. The titanite from granodiorite has REE content higher than those from MME and shows weak positive or negative Eu anomaly on REE pattern. It is indicate that the granitic melts of the Tongshanling are characterized by high oxygen fugacity (The chondrite values are from Sun and McDonough[31]).

榍石具有微弱的重稀土富集,La_N/Yb_N 比值为 0.12~0.85,具有明显的 Eu 正异常,Eu/Eu^* 值为 1.13~3.94;而花岗闪长岩中榍石稀土配分模式变化较大,Eu 正异常变小,部分分析点显示出负异常,Eu/Eu^* 值为 0.62~1.39。两类样品中榍石的微量元素对 Zr/Hf、Nb/Ta、Y/Ho 比值变化范围较小(表 2),Zr/Hf 比值为 21.0~31.5,Nb/Ta 比值为 10.4~13.9,Y/Ho 比值为 27.4~35.0。

表 1　铜山岭花岗闪长岩和暗色包体中榍石电子探针分析数据

Table 1　Representative EPMA data of titanite in granodiorite and mafic microgranular enclave of the Tongshanling pluton

元素/分析点	暗色包体(%)					花岗闪长岩(%)					
	TSL4-1	TSL4-2	TSL4-3	TSL4-4	TSL4-5	TSL5-1	TSL5-2	TSL5-3	TSL5-4	TSL5-5	TSL5-6
Na_2O	0.014	0.013	–	0.056	0.009	–	–	0.003	–	–	–
K_2O	0.009	0.004	0.001	0.006	0.008	–	–	–	–	–	–
F	1.45	0.48	1.45	1.69	1.23	1.84	0.255	1.57	1.10	1.09	1.07
MgO	–	0.003	0.001	–	0.005	0.031	0.001	0.017	–	–	0.002
Al_2O_3	3.62	2.70	3.60	4.14	3.31	5.61	1.81	4.68	3.03	3.37	2.48
SiO_2	31.7	31.4	31.2	31.3	30.7	31.3	31.1	31.4	31.6	31.0	31.6
Cl	0.017	–	0.008	0.012	0.002	0.005	–	–	0.007	–	0.004
CaO	29.4	29.3	30.0	29.9	29.4	29.9	29.6	29.0	29.6	29.5	29.4
TiO_2	33.9	35.7	35.1	33.7	34.0	30.6	38.2	32.9	35.0	34.2	36.8
MnO	0.059	0.043	0.024	0.045	0.061	0.028	0.044	0.053	0.066	0.024	0.027
FeO	0.220	0.356	0.366	0.190	0.184	0.465	0.378	0.191	0.606	0.456	0.432
总计	100	99.9	102	101	98.9	99.7	101	99.8	101	99.7	102
以 O=5 计算的阳离子个数(afpu)											
Na	0.001	0.001	–	0.003	0.001	–	–	–	–	–	–
Mg	–	–	–	–	–	0.001	–	0.001	–	–	–
Al	0.069	0.052	0.068	0.078	0.064	0.107	0.034	0.089	0.057	0.065	0.047
Si	1.021	1.020	0.996	1.004	1.008	1.013	1.001	1.015	1.016	1.010	1.007
Ca	1.013	1.020	1.026	1.025	1.032	1.038	1.020	1.002	1.020	1.030	1.006
Ti	0.822	0.872	0.841	0.812	0.840	0.745	0.925	0.800	0.847	0.839	0.883
Mn	0.002	0.001	0.001	0.001	0.002	0.001	0.001	0.001	0.002	0.001	0.001
Fe	0.006	0.010	0.010	0.005	0.005	0.013	0.010	0.005	0.016	0.012	0.012
F	0.008	0.003	0.008	0.009	0.007	0.010	0.001	0.008	0.006	0.006	0.006
F 和 Cl	0.001	–	–	0.001	–	–	–	–	–	–	–
Al+Fe	0.075	0.061	0.078	0.083	0.069	0.120	0.044	0.094	0.074	0.077	0.058

注:"–"代表低于检测限,下同。

表 2　铜山岭花岗闪长岩和暗色包体中榍石原位微量元素组成

Table 2　Trace element compositions of titanite in granodiorite and mafic microgranular enclave of the Tongshanling pluton

元素/分析点	暗色包体(μg/g)					花岗闪长岩(μg/g)					
	TSL4-1	TSL4-2	TSL4-3	TSL4-4	TSL4-5	TSL5-1	TSL5-2	TSL5-3	TSL5-4	TSL5-5	TSL5-6
Li	0.431	0.565	0.141	0.264	0.050	1.17	–	0.082	0.260	0.942	–
V	1461	571	610	1317	701	781	553	643	687	795	717
Ni	0.178	0.560	0.417	0.032	0.619	0.042	0.185	0.431	–	0.338	–
Cu	0.532	0.510	0.589	0.329	0.761	0.648	0.596	0.265	0.357	0.347	0.651
Zn	2.22	2.36	3.49	1.91	2.59	1.76	1.02	2.94	1.15	2.21	1.31
Ga	8.27	6.41	6.58	7.61	6.31	3.56	3.88	7.71	7.68	2.23	6.38
As	0.776	2.36	0.632	0.365	2.66	7.54	1.51	2.63	3.80	3.25	0.796
Rb	0.063	0.742	0.088	–	0.003	0.242	0.051	0.033	0.137	0.087	0.099
Sr	4.66	6.61	6.16	4.74	6.29	7.23	7.51	6.22	7.62	11.3	6.42
Y	270	74.0	131	32.4	90.9	118	872	333	1706	74.9	906
Zr	16.5	143	26.8	59.4	486	11.1	154	190	536	474	67.0
Nb	384	584	354	306	1489	650	625	1069	1455	1217	963
Sn	861	4116	3960	1353	6594	90	1162	3503	1233	829	651
Cs	0.112	0.320	0.038	0.039	0.004	0.317	0.002	0.005	0.044	0.110	0.011
Ba	0.093	0.342	0.055	0.108	0.053	1.323	–	0.080	0.033	1.263	0.048
La	5.33	9.87	8.07	4.19	5.92	16.5	4.37	14.1	15.8	15.7	2.75

（续表 2）

元素/分析点	暗色包体(μg/g)					花岗闪长岩(μg/g)					
	TSL4-1	TSL4-2	TSL4-3	TSL4-4	TSL4-5	TSL5-1	TSL5-2	TSL5-3	TSL5-4	TSL5-5	TSL5-6
Ce	24.8	43.1	48.4	16.6	21.5	63.9	43.2	73.9	98.1	51.4	25.7
Pr	5.45	6.39	9.19	2.58	3.91	11.9	15.5	15.8	27.0	7.02	9.56
Nd	37.6	29.6	49.9	13.1	24.9	69.8	135.2	97.8	214	32.6	86.8
Sm	19.8	7.79	13.2	4.95	10.7	22.2	86.8	35.8	135	26.4	68.5
Eu	8.94	10.9	13.4	5.71	15.7	10.2	46.0	17.4	32.5	28.8	20.3
Gd	29.7	9.59	16.2	5.09	13.8	22.6	118	42.2	192	25.9	108
Tb	5.95	1.58	2.85	0.84	2.18	3.50	21.7	7.20	37.03	1.42	21.3
Dy	42.7	10.5	19.8	5.3	13.3	20.1	143	47.5	259	9.8	151
Ho	9.84	2.45	4.44	1.12	3.05	4.20	30.2	10.9	55.4	2.14	31.2
Er	29.0	7.2	13.5	3.3	9.0	11.0	85.5	33.9	166.4	6.5	89.3
Tm	4.63	1.18	2.21	0.51	1.40	1.58	13.73	5.69	26.6	1.12	13.6
Yb	32.1	10.3	17.2	3.5	9.8	10.1	103	47.5	206	10.8	100
Lu	4.52	1.97	3.38	0.52	1.29	1.49	17.3	9.48	33.0	1.91	14.1
Hf	0.639	5.09	0.849	2.10	19.0	0.387	7.36	6.77	21.0	16.4	2.13
Ta	28.4	52.1	34.0	24.7	109.5	56.0	56.2	85.7	104.8	91.0	80.3
W	10.2	167	50.5	13.3	173	11.1	3.24	609	366	144	6.15
Pb	0.495	1.386	0.502	0.280	1.14	5.52	0.540	1.43	1.39	1.68	0.427
Th	2.13	3.76	1.44	6.40	2.52	2.35	5.04	63.5	62.0	6.92	2.41
U	17.2	52.8	16.9	18.2	19.8	4.39	18.0	262	205	45.4	10.1
ΣREE	258	152	222	67	136	269	864	459	1498	187	742
La_N/Yb_N	0.12	0.69	0.34	0.85	0.43	1.17	0.03	0.21	0.06	1.04	0.02
T(℃)	762	878	786	828	956	743	883	895	963	954	834
Eu/Eu^*	1.13	3.86	2.80	3.48	3.94	1.39	1.39	1.37	0.62	1.10	0.72
Ce/Ce^*	1.13	1.33	1.38	1.24	1.09	1.12	1.29	1.22	1.17	1.20	1.23
Zr/Hf	25.9	28.1	31.5	28.3	25.6	28.7	21.0	28.0	25.5	29.0	31.4
Nb/Ta	13.5	11.2	10.4	12.4	13.6	11.6	11.1	12.5	13.9	13.4	12.0
Y/Ho	27.4	30.2	29.6	28.8	29.8	28.0	28.9	30.7	30.8	35.0	29.0

3.2　榍石 Sm-Nd 同位素特征

3 个样品中榍石的微区原位 Sm-Nd 同位素分析结果见表 3。单颗粒榍石的 Sm-Nd 同位素组成非常均一，暗色包体中榍石的$^{147}Sm/^{144}Nd$ 比值为 0.2399～0.4026，$^{144}Nd/^{143}Nd$ 变化范围为 0.512321～0.512675，$\varepsilon_{Nd}(t)$值为-3.5～-8.9，平均值为-7.2±2.4。花岗闪长岩中榍石$^{147}Sm/^{144}Nd$ 比值为 0.2850～1.4020，$^{144}Nd/^{143}Nd$ 变化范围为 0.512269～0.513399，$\varepsilon_{Nd}(t)$值为-5.4～-9.9，平均值为-6.9±2.4。花岗闪长岩中榍石的 Sm-Nd 同位素比值变化范围略大于暗色包体中榍石的 Sm-Nd 同位素比值，但两者的初始 Nd 同位素组成非常相似（图 4）。

表 3　榍石原位 Sm-Nd 同位素组成

Table 3　*In-situ* Sm-Nd isotope compositions in titanite from granodiorite and mafic microgranular enclave of the Tongshanling pluton

暗色包体分析点	$^{147}Sm/^{144}Nd$	2σ	$^{143}Nd/^{144}Nd$	2σ	$\varepsilon_{Nd}(t)$	2σ	$f_{Sm/Nd}$	2σ
T4TNd07	0.3415	0.0099	0.512337	0.000442	-8.9	0.6	0.736	0.050
T4TNd09	0.3894	0.0010	0.512392	0.000095	-8.8	1.9	0.980	0.005
T4TNd10	0.4026	0.0026	0.512675	0.000057	-3.5	1.1	1.047	0.013
T4TNd11	0.2416	0.0048	0.512321	0.000283	-7.1	1.5	0.228	0.024
T4TNd12	0.2399	0.0072	0.512504	0.000744	-3.5	1.5	0.220	0.037
T4TNd13	0.2626	0.0018	0.512346	0.000509	-7.0	0.9	0.335	0.009
花岗闪长岩分析点	$^{147}Sm/^{144}Nd$	2σ	$^{143}Nd/^{144}Nd$	2σ	$\varepsilon_{Nd}(t)$	2σ	$f_{Sm/Nd}$	2σ
T3TNd01	1.4020	0.0098	0.513399	0.000267	-9.9	1.2	6.127	0.050
T5TNd01	0.4059	0.0026	0.512580	0.000166	-5.4	1.2	1.063	0.013
T5TNd02	0.5917	0.0046	0.512761	0.000140	-5.7	0.7	2.008	0.023
T5TNd05	0.3743	0.0047	0.512404	0.000270	-8.2	1.3	0.903	0.024
T3TNd03	0.2850	0.0048	0.512269	0.000693	-9.0	3.5	0.449	0.024

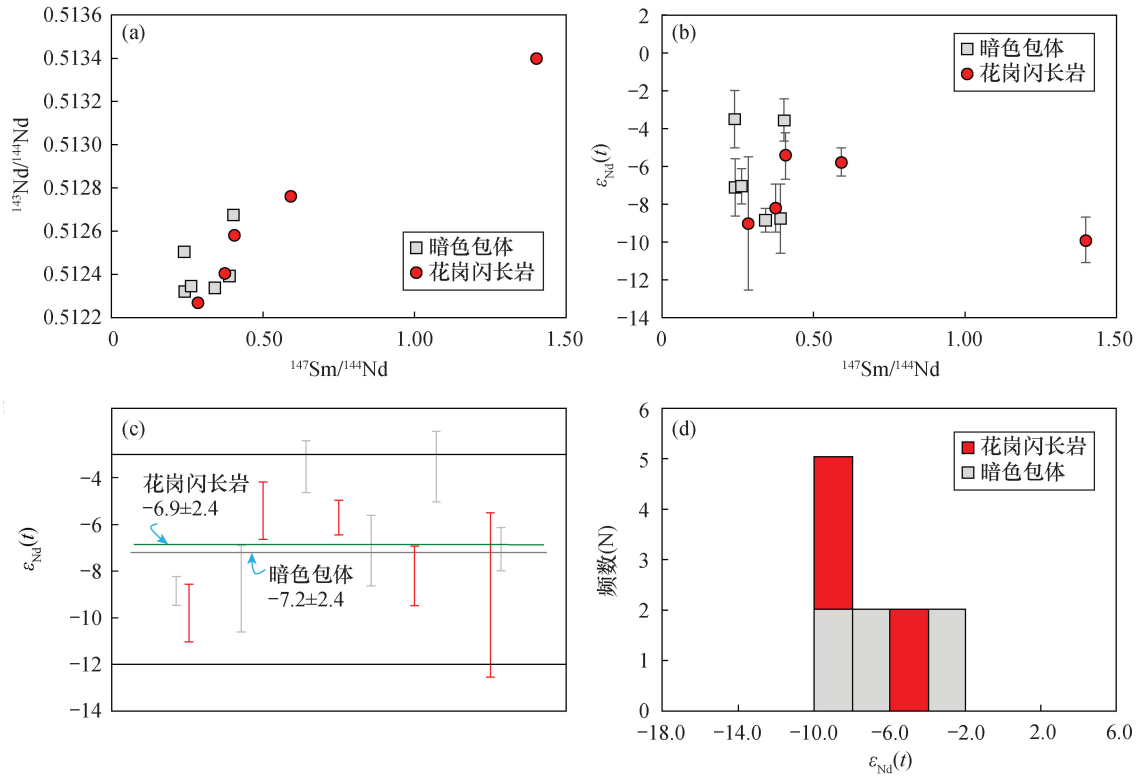

a—榍石 $^{147}Sm/^{144}Nd$ 与 $^{143}Nd/^{144}Nd$ 相关图; b—榍石 $^{147}Sm/^{144}Nd$ 与 $\varepsilon_{Nd}(t)$ 相关图; c—榍石 $\varepsilon_{Nd}(t)$ 加权平均值; d—榍石 $\varepsilon_{Nd}(t)$ 柱状图。

图 4　铜山岭花岗闪长岩和暗色包体中榍石 Sm−Nd 同位素组成,暗色包体和花岗闪长岩中的榍石具有相似的初始 Nd 同位素组成

Fig. 4　The Sm−Nd isotope compositions of titanite from the Tongshanling granitic pluton. All titanite grains have coincident negative initial Nd isotopic compositions. (a) Plot of $^{147}Sm/^{144}Nd$ against $^{143}Nd/^{144}Nd$ for titanite; (b) Plot of $^{147}Sm/^{144}Nd$ against $\varepsilon_{Nd}(t)$ for titanite; (c) Weighted mean ε_{Nd} value(t) for titanite; (d) Histogram of $\varepsilon_{Nd}(t)$ value for titanite. Titanite from MME has homogenous Nd isotope compositions. Their present $^{144}Nd/^{143}Nd$ ranges from 0.512321 to 0.512675, corresponding to $\varepsilon_{Nd}(t)$ value from −3.5 to −8.9 with an average of −7.2±2.4 (N=6). Titanite from granodiorite overall have $^{144}Nd/^{143}Nd$ ratio ranging from 0.512269 to 0.513399. Their time−corrected initial $\varepsilon_{Nd}(t)$ value vary between −5.4 and −9.9 with an average of −6.9±2.4 (N=5). All titanite grains have negative initial Nd isotopic compositions.

4　榍石地球化学特征对岩石成因的指示

4.1　榍石形成条件及其对岩浆性质的约束

副矿物榍石主量元素通常存在较大的差异,且含有较高的稀土元素和高场强元素,常被应用于判别榍石成因进而揭示寄主岩石的形成条件。因此,元素在榍石晶格位的替代方式得到了地质学者的广泛关注[32]。铜山岭花岗闪长岩及其中暗色包体中榍石普遍含有 Al、Fe 和 F 等元素,具有相似的元素变化趋势,Al+Fe 与 Ti 具有明显的负相关关系(图 5a),暗示 Al 和 Fe 主要通过替代八面体位置上的 Ti 进入榍石,具体的替代方式是 $(Al, Fe^{3+})+(F, OH)=Ti^{4+}+O^{2-}$。然而,在 Al+Fe 和 F 的关系图中,Al 和 Fe 超过了 $(Al, Fe^{3+})+(F, OH)=Ti^{4+}+O^{2-}$ 理论替换线(图 5b),说明还有额外的 Al 通过替换进入榍石晶格。铜山岭花岗闪长岩及暗色包体中榍石具有较高的 REE 含量,很可能还发生了 Al+Fe+REE 一起替换了 Ti 位和 Ca 位,替代方式是 $(Al, Fe^{3+})+REE=Ti^{4+}+O^{2-}$。因此,榍石中微量元素可能同时通过上述两种替代方式进入其晶格中。

元素进入榍石晶格与其形成条件密切相关[33-35]。一般而言,岩浆成因榍石具有低 CaO 和 TiO_2 含量,高 FeO、Na_2O 和 MgO 含量,稀土和高场强元素含量较高,稀土元素配分模式呈现出平坦的中−重稀土型式,这些地球化学特征明显有别于热液和变质成因的榍石[36-37,35]。当有流体参与作用时,矿物中的等价微量元素对 Zr−Hf、Nb−Ta 和 Y−Ho 会发生明显分异,偏离地壳岩石的正常范围[38-40],由于流体作用中,这些元素在矿物和熔体

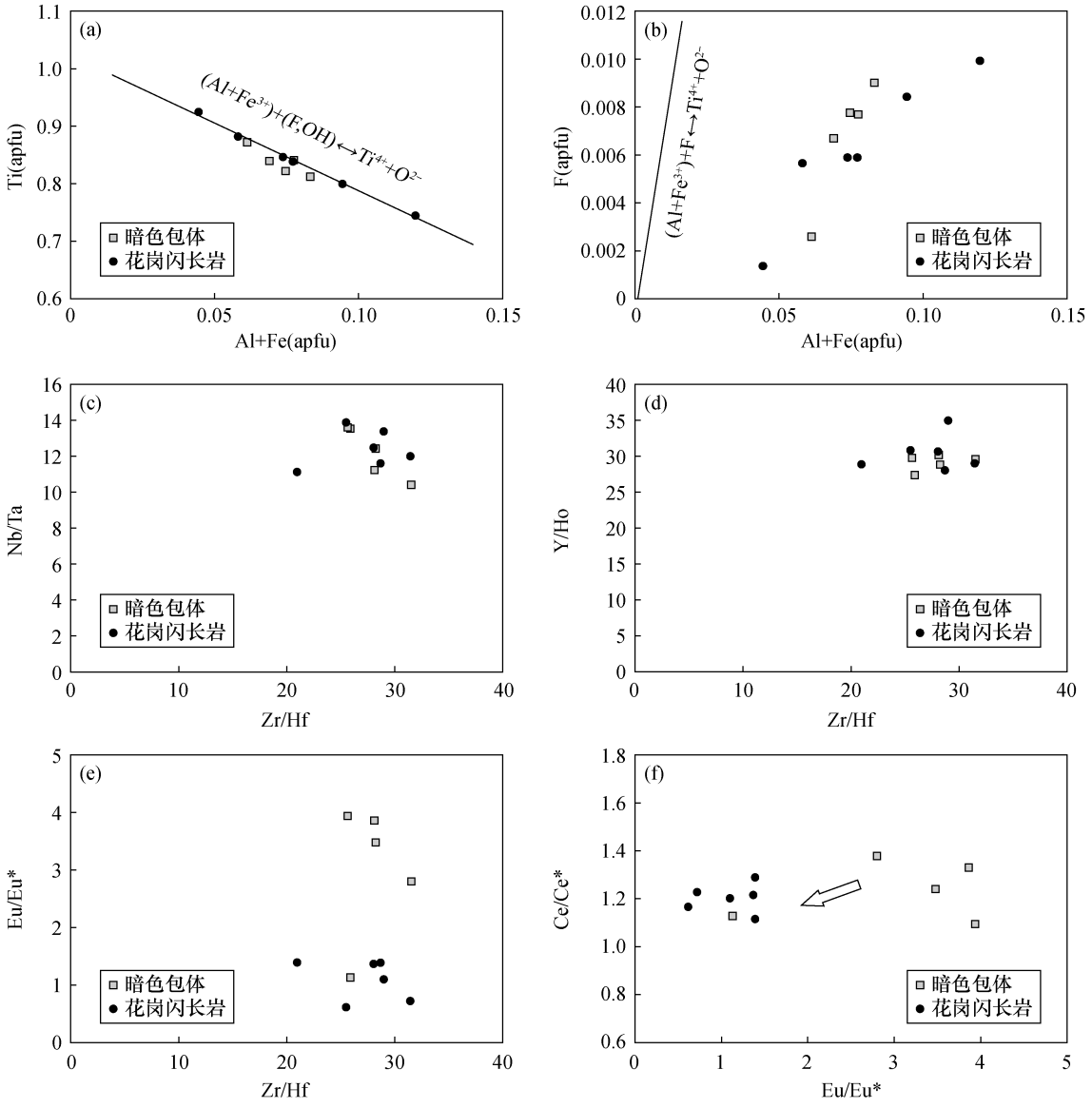

a—Ti 和 Al+Fe 相关图；b—F 和 Al+Fe 相关图；c—Zr/Hf 比值和 Nb/Ta 比值相关图；d—Zr/Hf 比值和 Y/Ho 比值相关图；e—Eu 异常 Eu/Eu* 和 Zr/Hf 比值相关图；f—Eu 异常 Eu/Eu* 和 Ce 异常 Ce/Ce* 相关图。

图 5　铜山岭榍石主量元素(a,b)和微量元素比值(c,d,e,f)相关图。榍石中主微量元素受离子半径和电荷控制,不受热液活动的影响,能反映初始岩浆的信息

Fig. 5　Selected major element variational diagrams (a, b) and trace element ratios variational diagrams (c-f) for titanite. The variation of Zr/Hf, Nb/Ta and Y/Ho ratios of titanite grains range from 21.0 to 31.5, 10.4 to 13.9 and 27.4 to 35.0, respectively. These trace element ratios are consistent with those of normal crust and are not fractionated. Therefore, the trace elements of titanite were completely controlled by ion radius and charge, and not affected by late hydrothermal alteration.

之间的分配不再受电价和离子半径控制[41]。铜山岭花岗闪长岩与铜多金属成矿在时空和成因上密切相关，岩体普遍遭受了强烈的热液蚀变作用[25,27-28]，热液活动是否对榍石的形成存在影响目前尚不明确。本次研究的榍石具有平坦的中-重稀土元素配分模式(图 3)，与苏鲁大别超高压变质岩中残留岩浆榍石的稀土配分模式完全一致[34]。所有榍石均具有低的 CaO、Al_2O_3 和 TiO_2 含量及高的 Fe_2O_3 和 MgO 含量(表 1)，元素的含量也与苏鲁大别超高压变质岩中残留岩浆榍石及三江地区碱性岩中岩浆榍石的元素含量相当[36,34-35]。这些元素地球化学特征均说明所研究的榍石都属于岩浆成因。而且，铜山岭花岗闪长岩和暗色包体中榍石中 Nb/Ta、Zr/Hf 和 Y/Ho 比值变化范围非常小(图 5)，

Nb/Ta 比值一般小于 13.5,Zr/Hf 比值一般大于 21,Y/Ho 比值大于 27.4,完全处于离子半径和电价控制的范围。因此,榍石未受热液活动的影响,保持岩浆初始信息,可以用于限定寄主岩石的岩浆性质。

已有实验研究表明,微量元素 Zr 可以取代榍石中的 Ti,其取代量的多少与体系的温度和压力相关,因此,榍石被广泛应用于地质温压条件的估算[42-44]。系统的实验研究证实,榍石中 Zr 含量与温压条件存在以下关系式[42]:

$$\log(Zr_{榍石}) = 10.52(\pm0.10) - 7708(\pm101)/T - 960(\pm10)P/T - \log(\alpha_{TiO_2}) - \log(\alpha_{SiO_2})$$

式中:$Zr_{榍石}$ 为榍石中 Zr 含量(μg/g);T 为温度(K);P 为压力(GPa),α_{TiO_2} 和 α_{SiO_2} 分别为 Ti 和 Si 的活度。

前人通过角闪石的 Al 压力计获得了铜山岭花岗闪长岩形成的压力约为 2.0GPa[22]。由于铜山岭花岗闪长岩中含有金红石和石英,假定 α_{TiO_2} 和 α_{SiO_2} 均为 1,即 Ti 和 Si 的活度均为 1,根据榍石中 Zr 含量,计算得到暗色包体中榍石的形成温度为 762~956℃,略高于花岗闪长岩中榍石的形成温度 743~963℃(表 2),并明显高于前人通过角闪石、黑云母和斜长石等矿物计算的温度[22]。因此,榍石记录的是初始岩浆温度条件,暗色包体中的榍石形成时间略早于寄主花岗岩闪长中的榍石。根据 Chappell 等[45]提出的高温和低温花岗岩类分类标准,铜山岭花岗闪长岩属于高温花岗岩类。同时,榍石中 Ce 和 Eu 异常通常与岩浆氧化还原状态密切相关,由于不同的氧化还原条件下,Ce 可以 Ce^{3+} 和 Ce^{4+},Eu 可以 Eu^{2+} 和 Eu^{3+} 存在[46,35]。还原条件下,Ce 主要以低价态的 Ce^{3+} 形式存在,Ce^{3+} 离子半径为 1.02Å,与 7 次配位 Ca^{2+} 离子半径 1.06Å 相似,容易置换榍石中的 Ca^{2+} 进入晶格,从而导致较高的 Ce/Ce^* 比值;而 Eu 主要以 Eu^{2+} 形式存在,Eu^{2+} 离子半径为 1.17 Å,与榍石中 7 次配位 Ca^{2+} 离子半径相差较大,难以置换进入榍石晶格,从而具有较低的 Eu/Eu^* 比值[46]。氧化条件下,榍石中 Ce/Ce^* 比值和 Eu/Eu^* 比值则反之。铜山岭花岗闪长岩暗色包体中榍石具有 Eu 的正异常,而花岗闪长岩中榍石分析点大部分显示出 Eu 的弱负异常,少量点具有 Eu 正异常(图 3),Eu/Eu^* 比值降低(图 5),二者的 Ce/Ce^* 比值都大于 1.0,且与 Eu/Eu^* 比值变化存在相关性(图 5)。因此,榍石中 Eu、Ce 异常说明岩浆的初始氧逸度较高,随着岩浆演化,氧逸度有降低趋势。

4.2　榍石 Nd 同位素对岩浆源区示踪

铜山岭花岗闪长岩具有明显的富钾、高铝特征[47,28],全岩初始 Sr-Nd 同位素变化范围较大,初始 $^{87}Sr/^{86}Sr$ 变化范围为 0.707962~0.710396,$\varepsilon_{Nd}(t)$ 值为-2.3~-7.0[47,28]。基于全岩 Sr-Nd 同位素和元素特征,前人认为铜山岭花岗闪长岩主要由壳幔物质混合形成或者残留体再造[45-46]。由于花岗质岩石在风化和热液蚀变过程中 Sm-Nd 同位素体系容易重置,难以限定岩浆源区特征,而榍石抗风化抗热液蚀变能力强,其原位 Sm-Nd 同位素代表了榍石结晶时岩浆的 Nd 同位素组成,可以有效地示踪岩浆来源和演化过程物质的变化细节,榍石原位 Nd 同位素成为了示踪岩浆源区和演化过程一个新的有效手段[15,14,35]。铜山岭花岗闪长岩中暗色包体的榍

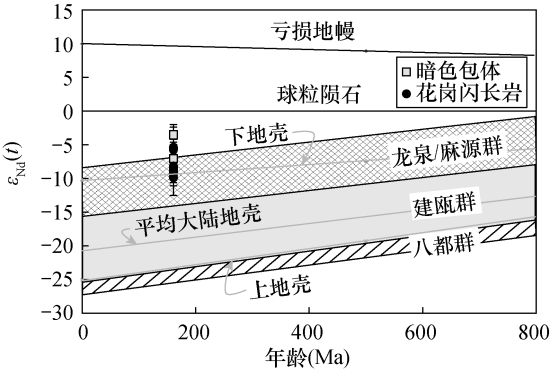

图 6　铜山岭榍石 Nd 同位素演化曲线。铜山岭榍石的初始 Nd 同位素靠近华南中下地壳 Nd 同位素演化线,暗示铜山岭花岗闪长质岩石的物质源区是华南中下地壳物质。所有初始同位素比值根据年龄 159±1Ma 进行校正,华南中下地壳 Sr-Nd 同位素数据据 Yu 等[49]和孔华等[48],元古代中基性变质岩数据据袁忠信等[50],Nd 同位素演化曲线据 Chen 等[51]

Fig. 6　Nd isotopic evolution diagrams for titanite from the Tongshanling granodiorite. All titanite grains have negative initial Nd isotopic compositions, which is consistent with the evolution trend of Nd isotopes of the middle-lower continental crust of South China. It is indicated that granodiorites from the Tongshanling pluton were probably formed by the amphibole-dehydration melting of a mafic source in the middle-lower crust beneath South China. All the initial ratios were corrected to 159±1Ma. The Nd isotopic data of middle/lower crust are from Yu, et al[49] and Kong, et al[48]. The data of Proterozoic metamorphic rocks are from Yuan, et al[50]. Nd isotopic evolution diagram was modified after Chen, et al[51].

石 $\varepsilon_{Nd}(t)$ 值为-3.5~-8.9,平均值为-7.2±2.4,花岗闪长岩中榍石 $\varepsilon_{Nd}(t)$ 值为-5.4~-9.9,平均值为-6.9±2.4,二者变化范围相似(图 4),而且同一颗粒不同生长环带的 Nd 同位素组成比较均一,说明在榍石结晶过程中岩浆来源没有发生明显变化,没有明显的岩浆混合特征。

在 Nd 同位素演化曲线上,铜山岭花岗闪长岩和暗色包体中榍石都具有负的初始 Nd 同位素组成,靠近华南大陆中下地壳 Nd 同位素区域,与湘南地区下地壳麻粒岩包体的 Nd 同位素组成相似[$\varepsilon_{Nd}(t)$ 值为-6.59~-7.34][48],处于元古代麻源群中基性变质岩的范围(图 6)。因此,铜山岭地区的花岗闪长岩很可能由均一的镁铁质中下壳熔融形成。然而,中下地壳什么样的物质能产生富钾、富铝的岩浆?前人通过实验研究发现,角闪岩脱水熔融过程产生的水不饱和岩浆具有高铝、高钾特征,而产生的水饱和岩浆具有高铝、高钙,但亏损铁、镁和钾特征[52-53],因此,铜山岭岩体很可能由镁铁质角闪岩相中下地壳发生脱水熔融形成的水不饱和岩浆形成。

5　结论

利用 LA-ICP-MS 和 LA-MC-ICP-MS 等现代原位分析测试技术,精确测定了铜山岭岩体中镁铁质暗色包体(MME)和寄主花岗闪长岩中副矿物榍石的微量元素和 Nd 同位素组成,确定了 REE 与 Al 和 Fe 主要通过 $(Al,Fe^{3+})+REE=Ti^{4+}+O^{2-}$ 方式替换榍石的 Ti 位和 Ca 位而进入晶格。榍石中微量元素对 Zr/Hf、Nb/Ta、Y/Ho 比值变化范围完全受控于离子半径和电荷,不受热液蚀变的影响,保留岩浆初始信息。榍石原位化学组成对示踪岩浆性质和起源具有明显的优势。

榍石微量元素分析结果表明铜山岭花岗闪长质岩浆初始氧逸度高,随岩浆演化有降低趋势。暗色包体和寄主花岗闪长岩中榍石具有均一的、负的 Nd 同位素组成,变化范围较小,与华南大陆中下地壳 Nd 同位素演化趋势一致,暗示铜山岭花岗闪长岩很可能由镁铁质角闪岩相中下地壳脱水熔融形成的水不饱和岩浆形成。

Petrogenesis of the Mesozoic Tongshanling Granodiorite in Southern Hunan Province, South China: Clues from *in-situ* Nd Isotopes and Elements of the Titanite

WANG Dan, *FU Yong**

(College of Resource and Environmental Engineering, Guizhou University, Guiyang 550025, China)

HIGHLIGHTS

(1) The elemental composition of Tongshanling titanite is controlled by the crystal structure, which records the initial information of magma.

(2) The granitic melts of the Tongshanling are characterized by high temperature and oxygen fugacity.

(3) The granodiorite of the Tongshanling pluton was produced by the amphibole-dehydration melting of a mafic source in the middle-to-lower crust.

ABSTRACT

BACKGROUND: The compositions of the bulk-rocks are commonly modified by hydrothermal alteration or merely represent the magmatic information of snapshot during evolution. Hence, use of the chemical compositions of bulk-rocks makes it difficult to trace the source and evolution of granitic magmas. The petrogenesis of the granitic rock is therefore difficult to decipher. In the face of these difficulties, an alternative new approach is to trace the magmatic source and evolution by *in-situ* analyzing elements and isotope compositions of accessory minerals in granitic rocks. This new approach can significantly improve the spatial resolution of the magmatic processes. Titanite ($CaTiSiO_5$)

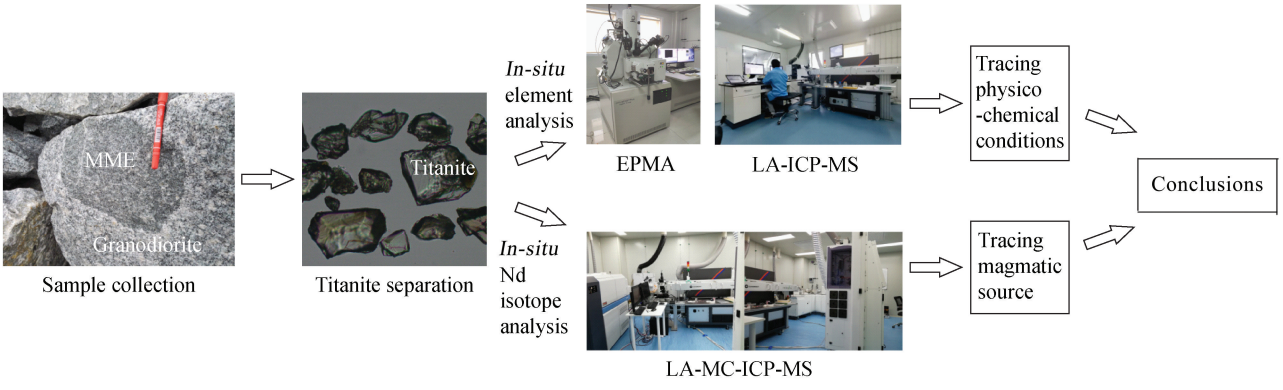

is a common accessory mineral of granitic rocks and contains a large amount of elements, including Al, Fe, Nb, Ta, Zr, Cr, V, Sn in the Ti site, and rare earth elements (REEs) Y, Na, Mn, Pb, U, Th, Sr and Ba in the Ca site. REEs and high field strength elements (HFSEs, i. e., Nb, Ta, Zr, Th and U) in titanite are sensitive to the changes of temperature, pressure, oxygen fugacity (f_{O_2}), water fugacity and melt composition. Additionally, titanite has high Nd concentration and low Sm/Nd ratio and is suitable for *in-situ* Nd isotope analyses. Therefore, titanite is an ideal accessory mineral to be used to investigate the magmatic source and evolution of granitic rocks.

OBJECTIVES: To trace the magmatic source and evolution, and to decipher the petrogenesis of the granitic rock.

METHODS: Titanite from mafic microgranular enclave (MME) and hosted granodiorite of the Tongshanling granitic pluton were checked by transmission light and back-scattered electron (BSE). BSE images were performed at the Institute of Geochemistry, Chinese Academy of Sciences (IGCAS) in Guiyang, on carbon-coated, polished epoxy blocks using JSM-7800F field emission scanning electron microscopy (SEM) operated at 20kV accelerating voltage and a beam current of 10nA. Their *in-situ* major element compositions were analysed by electron probe microanalyzer (EPMA) at IGCAS. An accelerating voltage of 25kV and a probe current of 10nA were applied. Well-characterized Kaersutite (Na, K, Mg, Al, Si, Ca, Mn, and Fe), apatite (F), and rutile (Ti) were used as standards. The trace elements of titanite were analysed *in-situ* by an Agilent 7900 ICPMS equipped with GeoLasPro 193nm ArF laser ablation system (LA-ICP-MS) at IGCAS. Analytical conditions were as follows: a fluence of 5J/cm^2, at a repetition rate of 5Hz and laser spot of 44μm. Ca (determined by EPMA) was chosen as the internal standard and the reference glasses NIST610 and NIST612 were used to calibrate relative element sensitivities. *In-situ* Nd isotope of titanite were analyzed by a Nu Plasma Ⅲ multi-collector (MC) equipped with RESOlution-155 ArF 193nm laser ablation system (LA-MC-ICP-MS) at IGCAS. Titanite was ablated in a mixture of helium (350mL/min) and nitrogen (2mL/min) atmosphere using the following parameters: 30s baseline time, 40s ablation time, 72μm spot size, 6Hz repetition rate and 6J/cm^2 energy density. The interference of ^{144}Sm on ^{144}Nd was derived from the ^{147}Sm intensity with a natural ^{144}Sm/^{147}Sm ratio of 0.205484. The mass bias factor of Sm was calculated from the measured isotopic ratio of ^{144}Sm/^{149}Sm and its true value 1.08680. The mass bias of ^{143}Nd/^{144}Nd was normalized to ^{146}Nd/^{144}Nd = 0.7129 with an exponential law. The reference materials MAD, Otter Lake, LAP and SAP were chosen as the external standards.

RESULTS: Titanite grains in the MME, and host granodiorite of the Tongshanling granitic pluton have similar major element compositions. All titanite are characterized by high SiO_2 (31.0% to 31.7%), CaO (29.0%-30.0%), TiO_2 (30.6%-38.2%), and low Al_2O_3 (1.81%-5.61%), FeO (0.184%-0.606%), F (0.48%-1.84%) contents. The MnO concentrations vary between 0.024% and 0.066%. The MgO concentrations range from 0.001% to 0.031%. Compositional zoning among single titanite grains were not observed. The crystallo-chemical formulae were calculated on the basis of 5 oxygen atoms. The calculated results indicate that the Al+Fe

(apfu) is negatively correlated with Ti (apfu) in all titanite grains. The analysed titanite grains have high rare earth element (REE) contents (67-1498μg/g). The REE were incorporated into titanite lattice by substituting for Ti and Ca site with Al and Fe and the substituted mechanism is $(Al,Fe^{3+})+REE=Ti^{4+}+O^{2-}$. On the REE patterns, the titanite from granodiorite has REE contents higher than that from MME and shows weak positive or negative Eu anomaly (Eu/Eu^{*} from 0.62 to 1.39). On the contrary, titanite from MME is characterized by Eu positive anomaly (Eu/Eu^{*} from 1.13 to 3.94). These titanite contain high content of HFSEs such as Zr (11.1-536 μg/g), Hf (0.639-21μg/g), Nb (306-1489μg/g) and Ta (24.7-109.5μg/g). The variation of Zr/Hf, Nb/Ta and Y/Ho ratios of titanite grains range from 21.0 to 31.5, 10.4 to 13.9 and 27.4 to 35.0, respectively. These trace element ratios are consistent with those of normal crust and are not fractionated. Therefore, the trace elements of titanite were completely controlled by ion radius and charge and not affected by late hydrothermal alteration. Titanite Zr thermometer shows that the temperature of titanite formation is between 762℃ and 963℃. Titanite from MME has homogenous Nd isotope compositions. Their present $^{144}Nd/^{143}Nd$ ranges from 0.512321 to 0.512675, corresponding to $\varepsilon_{Nd}(t)$ value from -3.5 to -8.9 with an average of -7.2±2.4 ($N=6$). Titanite from granodiorite overall have $^{144}Nd/^{143}Nd$ ratio ranging from 0.512269 to 0.513399. Their time-corrected initial $\varepsilon_{Nd}(t)$ value vary between -5.4 and -9.9 with an average of -6.9±2.4 ($N=5$). All titanite grains have negative initial Nd isotopic compositions, which is consistent with the evolution trend of Nd isotopes of the middle-lower continental crust of South China.

CONCLUSIONS: Titanite grains in the MME and host granodiorite of the Tongshanling granitic pluton show little or no intra-grain concentric zoning in BSE images and display similar element and isotopic geochemical characteristics. Crystal chemical exerts a first-order control on elemental compositions of titanite. Titanite survived during hydrothermal alteration and faithfully recorded the information of granitic melts. The granitic melts of the Tongshanling are characterized by high temperature and oxygen fugacity. Granodiorites from the Tongshanling pluton were probably formed by the amphibole-dehydration melting of a mafic source in the middle-lower crust beneath South China.

KEY WORDS: LA-MC-ICP-MS; *in-situ* isotope analysis; Nd isotope; trace elements; titanite; granodiorite; southern Hunan Province

参考文献

[1] Anne-Sophie M J, Pichavant M. Magmatic fraction-ation and the magmatic-hydrothermal transition in rare metal granites: Evidence from Argemela (central Portugal)[J]. Geochimica et Cosmochimica Acta, 2020, 289(15): 130-157.

[2] Lehmann B. Formation of tin ore deposits: A reassessment[J]. Lithos, 2020, 402-403(15): 105756.

[3] Sun W D, Zhang C C, Liang H Y, et al. The genetic association between magnetite-hematite and porphyry copper deposits: Reply to Pokrovski[J]. Geochimica et Cosmochimica Acta, 2014, 126: 639-642.

[4] Lackey J S, Valley J W, Hinke H J. Deciphering the source and contamination history of peraluminous magmas using $\delta^{18}O$ of accessory minerals: Examples from garnet-bearing plutons of the Sierra Nevada batholith[J]. Contributions to Mineralogy and Petrology, 2006, 151(1): 20-44.

[5] 吴福元,李献华,杨进辉,等. 花岗岩成因研究的若干问题[J]. 岩石学报, 2007, 23(6): 1217-1238.
Wu F Y, Li X H, Yang J H, et al. Discussions on the petrogenesis of granites[J]. Acta Petrologica Sinica, 2007, 23(6): 1217-1238.

[6] Li X H, Li W X, Wang X C, et al. Role of mantle-derived magma in genesis of early Yanshanian granites in the Nanling Range, South China: *In situ* zircon Hf-O isotopic constraints[J]. Science in China: Series D—Earth Sciences, 2009, 52(9): 1262-1278.

[7] Waight T E, Tørnqvist J B. Sr isotope zoning in plagio-clase from andesites at Cabo De Gata, Spain: Evidence for shallow and deep contamination[J]. Lithos, 2018,

308-309:159-167.

[8] Grimes C,Wooden J,Cheadle M,et al. "Fingerprinting" tectono-magmatic provenance using trace elements in igneous zircon[J]. Contributions to Mineralogy and Petrology,2015,170(5-6):1-26.

[9] Miles A J,Graham C M,Hawkesworth C J,et al. Apatite: A new redox proxy for silicic magmas? [J]. Geochimica et Cosmochimica Acta,2014,132:101-119.

[10] Emo R B,Smit M A,Schmitt M,et al. Evidence for evolved Hadean crust from Sr isotopes in apatite within Eoarchean zircon from the Acasta gneiss complex[J]. Geochimica et Cosmochimica Acta, 2018, 235: 450-462.

[11] Fisher C M,Bauer A M,Luo Y,et al. Laser ablation split-stream analysis of the Sm-Nd and U-Pb isotope compositions of monazite, titanite, and apatite—Improvements, potential reference materials, and application to the Archean Saglek Block gneisses[J]. Chemical Geology,2020,539:119493.

[12] McLeod G W,Dempster T J,Faithfull J W. Deciphering magma-mixing processes using zoned titanite from the ross of mull granite,Scotland[J]. Journal of Petrology, 2011,52(1):55-82.

[13] Bruand E,Storey C,Fowler M,et al. Oxygen isotopes in titanite and apatite, and their potential for crustal evolution research[J]. Geochimica et Cosmochimica Acta,2019,255:144-162.

[14] Zhao Z,Wang C Y,Wei B,et al. Elemental and Nd isotopic compositions of zoned titanite in mafic microgranular enclaves of the early Cretaceous Sanguliu granitic pluton in the North China Craton:Insights into magma mixing process[J]. Lithos, 2021, 392-393: 106138.

[15] Hammerli J,Kemp A I S,Spandler C. Neodymium isotope equilibration during crustal metamorphism revealed by *in situ* microanalysis of REE-rich accessory minerals[J]. Earth & Planetary Science Letters,2014, 392:133-142.

[16] Laurent O,Zeh A,Gerdes,A et al. How do granitoid magmas mix with each other? Insights from textures, trace element and Sr-Nd isotopic composition of apatite and titanite from the Matok pluton (South Africa)[J]. Contributions to Mineralogy and Petrology, 2017, 172(9):80.

[17] Yang Y H,Wu F Y,Yang J H,et al. Sr and Nd isotopic compositions of apatite reference materials used in U-Th-Pb geochronology[J]. Chemical Geology,2014, 385:35-55.

[18] Huang X,Lu J,Sizaret S,et al. Petrogenetic differences between the middle-late Jurassic Cu-Pb-Zn-bearing and W-bearing granites in the Nanling Range,South China:A case study of the Tongshanling and Weijia deposits in southern Hunan Province[J]. Science China:Earth Sciences,2017,60(7):1220-1236.

[19] Yang J H,Kang L F,Peng J T,et al. *In-situ* elemental and isotopic compositions of apatite and zircon from the Shuikoushan and Xihuashan granitic plutons: Implication for Jurassic granitoid-related Cu-Pb-Zn and W mineralization in the Nanling Range, South China[J]. Ore Geology Reviews,2018,93:382-403.

[20] Huang J C,Peng J T,Yang J H,et al. Precise zircon U-Pb and molybdenite Re-Os dating of the Shuikoushan granodiorite-related Pb-Zn mineralization,southern Hunan,South China[J]. Ore Geology Reviews,2015,71:305-317.

[21] Zhao P,Yuan S,Mao J,et al. Zircon U-Pb and Hf-O isotopes trace the architecture of polymetallic deposits: A case study of the Jurassic ore-forming porphyries in the Qin—Hang metallogenic belt,China[J]. Lithos, 2017,292:132-145.

[22] Huang X D,Lu J J,Sizaret S,et al. Reworked restite enclave:Petrographic and mineralogical constraints from the Tongshanling intrusion,Nanling Range,South China [J]. Journal of Asian Earth Sciences,2018,166:1-18.

[23] 王岳军,范蔚茗,郭锋,等. 湘东南中生代花岗闪长质小岩体的岩石地球化学特征[J]. 岩石学报,2001,17(1):169-175.
Wang Y J,Fan W M,Guo F,et al. Petrological and geochemical characteristics of Mesozoic granodioritic intrusions in southeast Hunan Province,China[J]. Acta Petrologica Sinica,2001,17(1):169-175.

[24] Wang Y,Fan W,Guo F. Geochemistry of early Mesozoic potassium-rich diorites-granodiorites in southeastern Hunan Province,South China:Petrogenesis and tectonic implications[J]. Geochemical Journal, 2003, 37(4): 427-448.

[25] 卢友月,付建明,程顺波,等. 湘南铜山岭铜多金属矿田成岩成矿作用年代学研究[J]. 大地构造与成矿学,2015,39(6):1061-1071.
Lu Y Y,Fu J M,Cheng S B,et al. Rock-forming and ore-forming ages of Tongshanling copper polymetallic ore-field in southern Hunan Province[J]. Geotectonica et

Metallogenia,2015,39(6):1061-1071.

[26] 王岳军,范蔚茗,郭锋,等. 湘东南中生代花岗闪长岩锆石 U-Pb 法定年及其成因指示[J]. 中国科学:D 辑,2001,31(9):745-751.
Wang Y J,Fan W M,Guo F,et al. Zircon U-Pb dating of the Mesozoic granitoids from southeastern Hunan Province [J]. Science in China (Series D),2001,31(9):745-751.

[27] 蔡应雄,谭娟娟,杨红梅,等. 湘南铜山岭铜多金属矿床成矿物质来源的 S,Pb,C 同位素约束[J]. 地质学报,2015,89(10):1792-1803.
Cai Y X,Tan J J,Yang H M,et al. The origin of ore-forming material in the Tongshanling Cu-polymetallic ore field in Hunan Province:Constrains from S-Pb-C isotopes[J]. Acta Geologica Sinica,2015,89(10):1792-1803.

[28] 袁顺达. 湘南铜山岭矿田玉龙矽卡岩型钼矿床辉钼矿 Re-Os 测年[J]. 地质论评,2013,59(Z1):393-394.
Yuan S D. Molybdenite Re-Os dating of the Yulong skarn-type Mo deposit from Tongshanling ore-filed in South Hunan Province[J]. Geological Revies,2013,59(Z1):393-394.

[29] Dubois J,Retali G,Cesario J. Isotopic analysis of rare earth elements by total vaporization of samples in thermal ionization mass spectrometry[J]. International Journal of Mass Spectrometry and Ion Processes,1992,120(3):163-177.

[30] Yang Y,Sun J,Xie L,et al. *In situ* Nd isotopic measurement of natural geological materials by LA-MC-ICPMS[J]. Chinese Science Bulletin,2008,53(7):1062-1070.

[31] Sun S S,McDonough W F. Chemical and isotopic systematics of oceanic basalts:Implications for mantle composition and processes[J]. Geological Society of London (Special Publications),1989,42(1):313-345.

[32] Perseil E A,Smith D C. Sb-rich titanite in the manganese concentrations at St. Marcel-Praborna,Aosta Valley,Italy:Petrography and crystal-chemistry[J]. Mineralogical Magazine,1995,59(397):717-734.

[33] Cao M,Qin K,Li G,et al. *In situ* LA-(MC)-ICP-MS trace element and Nd isotopic compositions and genesis of polygenetic titanite from the Baogutu reduced porphyry Cu deposit,western Junggar,NW China[J]. Ore Geology Reviews,2015,65(4):940-954.

[34] Xu L,Bi X,Hu R,et al. LA-ICP-MS mineral chemistry of titanite and the geological implications for exploration of porphyry Cu deposits in the Jinshajiang—Red River alkaline igneous belt,SW China[J]. Mineralogy and Petrology,2015,109(2):181-200.

[35] 马倩,杨岳衡,赵志丹,等. 云南哀牢山—红河剪切带新生代富碱侵入岩中榍石年代学和地球化学特征[J]. 岩石学报,2020,36(9):2751-2778.
Ma Q,Yang Y H,Zhao Z D,et al. Titanite geochronology and geochemistry of the Cenozoic alkali-rich intrusions in the Ailaoshan—Red River shear zone,Yunnan Province[J]. Acta Petrologica Sinica,2020,36(9):2751-2778.

[36] Gao X Y,Zheng Y F,Chen Y X,et al. Geochemical and U-Pb age constraints on the occurrence of polygenetic titanites in UHP metagranite in the Dabie orogen[J]. Lithos,2012,136-139:93-108.

[37] Storey C D,Jeffries T E,Smith M. Common lead-corrected laser ablation ICP-MS U-Pb systematics and geochronology of titanite[J]. Chemical Geology,2006,227(1-2):37-52.

[38] Ballouard C,Poujol M,Boulvais P,et al. Nb-Ta fractionation in peraluminous granites:A marker of the magmatic-hydrothermal transition[J]. Geology,2016,44(3):231-234.

[39] Bau M. Controls on the fractionation of isovalent trace elements in magmatic and aqueous systems:Evidence from Y/Ho,Zr/Hf,and lanthanide tetrad effect[J]. Contributions to Mineralogy and Petrology,1996,123(3):323-333.

[40] Breiter K,Škoda R. Zircon and whole-rock Zr/Hf ratios as markers of the evolution of granitic magmas:Examples from the Teplice caldera (Czech Republic/Germany)[J]. Mineralogy and Petrology,2017,111(4):435-457.

[41] Irber W. The lanthanide tetrad effect and its correlation with K/Rb,Eu/Eu*,Sr/Eu,Y/Ho,and Zr/Hf of evolving peraluminous granite suites[J]. Geochimica et Cosmochimica Acta,1999,63(3-4):489-508.

[42] Hayden L A,Watson E B,Wark D A. A thermobarometer for sphene (titanite)[J]. Contributions to Mineralogy and Petrology,2008,155(4):529-540.

[43] Seifert W,Kramer W. Accessory titanite:An important carrier of zirconium in lamprophyres[J]. Lithos,2003,71(1):81-98.

[44] 朱乔乔,谢桂青,蒋宗胜,等. 湖北金山店大型矽卡岩型铁矿热液榍石特征和原位微区 LA-ICPMS U-Pb 定年[J]. 岩石学报,2014,30(5):1322-1338.
Zhu Q Q,Xie G Q,Jiang Z S,et al. Characteristics and *in*

situ U-Pb dating of hydrothermal titanite by LA-ICPMS of the Jingshandian iron skarn deposit, Hubei Province [J]. Acta Petrologica Sinica, 2014, 30(5): 1322-1338.

[45] Chappell B W, White A J R, Williams I S, et al. Low- and high-temperature granites [J]. Earth & Environmental Science Transactions of the Royal Society of Edinburgh, 2004, 95(1-2): 125-140.

[46] King P L, Sham T K, Gordon R A, et al. Microbeam X-ray analysis of Ce^{3+}/Ce^{4+} in Ti-rich minerals: A case study with titanite (sphene) with implications for multivalent trace element substitution in minerals [J]. American Mineralogist, 2013, 98(1): 110-119.

[47] Jiang Y H, Jiang S Y, Dai B Z, et al. Middle to late Jurassic felsic and mafic magmatism in southern Hunan Province, southeast China: Implications for a continental arc to rifting [J]. Lithos, 2009, 107(3-4): 185-204.

[48] 孔华,金振民. 道县玄武岩中麻粒岩包体的岩石学及年代学 [J]. 长春科技大学学报, 2000, 30(2): 115-119.

Kong H, Jin Z M. Petrology and chronology of granulite xenolith in Daoxian County, Hunan Province [J]. Journal of Changchun University of Science and Technology, 2000, 30(2): 115-119.

[49] Yu J H, Xu X, O'Reilly S Y, et al. Granulite xenoliths from Cenozoic basalts in SE China provide geochemical fingerprints to distinguish lower crust terranes from the North and South China tectonic blocks [J]. Lithos, 2003, 67(1-2): 77-102.

[50] 袁忠信,吴良士,张宗清,等. 闽北麻源群 Sm-Nd、Rb-Sr 同位素年龄研究 [J]. 岩石矿物学杂志, 1991, 10(2): 127-132.

Yuan Z X, Wu L S, Zhang Z Q, et al. The Sm-Nd, Rb-Sr isotopic age-dating of Mayuan Group in northern Fujian [J]. Acta Petrologica et Mineralogica, 1991, 10(2): 127-132.

[51] Chen J, Jahn B M. Crustal evolution of southeastern China: Nd and Sr isotopic evidence [J]. Tectonophysics, 1998, 284(1): 101-133.

[52] Beard J, Lofgren G. Dehydration melting and water-saturated melting of Basaltic and Andesitic greenstones and amphibolites at 1, 3, and 6. 9kb [J]. Journal of Petrology, 1991, 32(2): 365-401.

[53] Wolf M, Wyllie P. Dehydration-melting of amphibolite at 10kbar: the effects of temperature and time [J]. Contributions to Mineralogy and Petrology, 1994, 115(4): 369-383.